PNAS
www.pnas.org

Supplementary Information for

Differentially synchronized spiking enables multiplexed neural coding

Milad Lankarany, Dhekra Al-Basha, Stéphanie Ratté, and Steven. A. Prescott

Corresponding author: Steven A. Prescott
Email: steve.prescott@sickkids.ca

This PDF file includes:

Supplementary methods
Figs. S1 to S5
References for SI reference citations

www.pnas.org/cgi/doi/10.1073/pnas.1812171116

SUPPLEMENTARY METHODS

In vivo recordings

Surgery. Adult male (230-300 g) Sprague Dawley rats (Charles River, Montreal, Quebec) were anesthetized with isoflurane (3% for induction, 2% for maintenance). The upper thoracic region was shaved and anesthetic cream (2.5% lidocaine, 2.5% prilocaine; AstraZeneca, Mississauga, ON) was applied to the shaved skin 10-15 min prior to surgery. To cannulate the jugular vein, a small incision (~10 mm) was made just below the left clavicle. The jugular vein was separated from surrounding tissue and two loose knots were made around it. Immediately after tightening the rostral knot, the vein was incised and saline-primed PE60 tubing (Becton Dickinson, Mississauga, ON) was inserted and fixed in position by tightening the second knot. After ensuring that there was no resistance to flow, saline was delivered at a rate of 0.5 ml/hr using a Legato 101 syringe pump (KD Scientific, Holliston, MA) and the incision was closed. Next, the trachea was exposed by making a midline incision (~ 25 mm) between the lower jaw and upper thorax. The trachea was incised below the larynx and PE240 tubing (Becton Dickinson) already connected to an Inspira ventilator (Harvard Apparatus, Saint-Laurent, QC) was inserted into the trachea and secured, and the incision was closed. The rat was ventilated at 85 breaths/min and tidal volume of 2 cc.

The rat was transferred to a stereotaxic frame (Narishige, Amityville, NY) and its head fixed with ear bars. The head was shaved and anesthetic cream applied before exposing the skull. A 3x3 mm window was made through the skull over the right primary somatosensory cortex (S1), 1-4 mm caudal and 2.5-5.5 mm lateral to bregma. Ear bars were removed and the skull was cemented to a custom-made head plate and whiskers on the left side were trimmed. Heart rate and oxygen level were monitored (Nonin, Plymouth, MN) and body temperature was maintained at 37˚C using a feedback-controlled heating pad (TR-200; Fine Science Tools, Foster City, CA). After giving a loading dose of fentanyl (10 μg/kg) and pancuronium bromide (1.6 mg/kg), both drugs were infused continuously at 10 μg/kg/hr and 1.6 mg/kg/hr, respectively.

Single unit extracellular recordings: All recordings were conducted in a dimly lit and quiet room. A multielectrode array comprising 4 shanks each with 4 recording sites (A4 type, NeuroNexus, Ann Arbor, MI) connected to an Omniplex data acquisition system (Plexon, Dallas, TX) was lowered into the S1 cortex. Isoflurane was discontinued while monitoring the animal. Signals were amplified, digitized at 40 kHz, and high-pass filtered at 300 Hz. Receptive fields were identified by gently touching the whisker pad with a paint brush or blunt probe. Recordings were obtained 2.5-3.5 mm caudal and 4-5.5 mm lateral to bregma, 1.4-1.8 mm deep (layer 5).

Once a receptive field (RF) was identified, a Model 300C-I force-feedback mechanical stimulator (Aurora Scientific, Aurora, Ontario) with 1 mm diameter-wide blunt plastic tip was positioned with a micromanipulator. The timing and force of all stimuli were controlled (and the resulting forced recorded) using a Power1401 computer interface and Signal v5 software (Cambridge Electronic Design). Triggers sent from Signal were used to sync stimulation with neural recordings. Spikes were sorted using the Plexon offline sorter. Spike times were exported to Matlab for analysis described below.

A total of 44 well isolated single units were recorded from 5 rats. Stimulus sequences (trials) were repeated ≥4 times per animal but, for those units selected (see below), 4 trials were randomly drawn from each so that each unit contributed equally to the final data set. To identify units responsive to whisker pad stimulation, the firing rate evoked by 10, 12.5 and 15 g stimulation was averaged and compared to the spontaneous firing at the start of that trial. Units whose evoked firing rate was significantly greater than the spontaneous firing rate ($p < 0.05$, paired *t*-test) were included for further analysis, resulting in a total of 17 units. Units were not selected on the basis of any information about spike timing.

***In vitro* recordings**

Slice preparation. In vitro recordings were conducted on adult (6-8 week old) mice of either sex derived by crossing Pvalb-2A-Cre-D mice (JAX #012358) with Ai32 mice (JAX #012569). Offspring express channelrhodopsin-2 in parvalbumin-expressing interneurons but experiments targeted pyramidal neurons and did not involve optogenetic stimulation. Mice were anesthetized with 3% isoflurane and decapitated as previously described (1). The brain was rapidly removed to ice-cold carbogenated (95% O_2 and 5% CO_2) sucrose-substituted artificial CSF (ACSF) containing (in mM) 252 sucrose, 2.5 KCl, 2 $CaCl_2$, 2 $MgCl_2$, 10 glucose, 26 $NaHCO_3$, 1.25 NaH_2PO_4, and 5 kynurenic acid. Coronal slices of primary somatosensory cortex (S1) were cut at 400 μm thickness using a VT-1000S microtome (Leica, Concord, Ontario) and were kept in regular ACSF (126 mM NaCl instead of sucrose and without kynurenic acid) at room temperature until recording. Slices were transferred to a recording chamber perfused with ACSF maintained at 31±1°C.

Patch clamp recordings. Pyramidal neurons in layer 5 of S1 were recorded in whole-cell mode with >70% series resistance compensation using an Axopatch 200B amplifier (Molecular Devices, Sunnyvale, CA). The pipette solution contained (in mM) 125 $KMeSO_4$, 5 KCl, 10 HEPES, and 2 $MgCl_2$, 4 ATP (Sigma), and 0.4 GTP (Sigma); pH was adjusted to 7.2 with KOH. Synaptic transmission was blocked via bath application of (in μM) 10 CNQX, 40 D-AP-5, and 6 gabazine

(Abcam, Toronto, Ontario). The same mixed signal was applied on each trial via current injection with or without added noise, which if present, differed across trials (see below). Responses were low-pass filtered at 2 kHz and digitized at 20 kHz using a Power1401 computer interface and Signal 5 software (Cambridge Electronic Design, Cambridge, UK).

To recreate the noisy, high-conductance state observed *in vivo* (2), irregularly fluctuating conductances generated by Ornstein-Uhlenbeck (OU) processes (g_{exc0} = 1 nS, g_{inh0} = 4 nS, σ_{exc} = 0.3 nS, σ_{inh} = 0.75 nS, τ_{exc} = 3 mS and τ_{inh} = 10 ms) were applied using dynamic clamp. Alternatively, noise was introduced as a fluctuating current modeled as an OU process (σ_{noise} = 10 pA, τ_{noise} = 5 mS). In either case, noisy input caused membrane potential fluctuations of ~2 mV and spontaneous spiking of ~5 spikes/s. The same mixed signal by different noise was applied for each 100 s-long trial. Other trials were conducted with the same mixed signal but without any added noise. Data were included from all cells in which ≥4 trials were completed for at least one condition. No more than 7 trials per condition were collected per cell. Data collection was stopped when the data set for each condition neared or exceeded 30 trials.

Simulations

Neurons were modeled as previously described (1) using equations adapted from Morris and Lecar (3):

$$C\frac{dV}{dt} = I_{\text{mixed}}(t) + I_{\text{noise}}(t) - \bar{g}_{\text{Na}} m_{\infty}(V)(V - E_{\text{Na}}) - \bar{g}_{\text{K}} w(V - E_{\text{K}}) - g_{\text{L}}(V - E_{\text{L}}) - \bar{g}_{\text{AHP}} z(V - E_{\text{K}}) - g_{\text{exc}}(V - E_{\text{exc}}) - g_{\text{inh}}(V - E_{\text{inh}}) \quad \text{(S1)}$$

$$dw/dt = \phi \frac{w(V) - w}{\tau_W(V)} \quad \text{(S2)}$$

$$dz/dt = \left(\frac{1}{1 + e^{(\beta_z - V)/\gamma_z}} - z \right) / \tau_z \quad \text{(S3)}$$

$$m_{\infty}(V) = 0.5\left[1 + \tanh\left(\frac{V - \beta_m}{\gamma_m}\right)\right] \quad \text{(S4)}$$

$$w_{\infty}(V) = 0.5\left[1 + \tanh\left(\frac{V - \beta_w}{\gamma_w}\right)\right] \quad \text{(S5)}$$

$$\tau_w(V) = 1/\cosh\left(\frac{V - \beta_w}{2\beta_w}\right) \quad \text{(S6)}$$

where $\bar{g}_{\mathrm{Na}}$ = 20 mS/cm^2, $\bar{g}_{\mathrm{K}}$ = 20 mS/cm^2, g_{L} = 2 mS/cm^2, $\bar{g}_{\mathrm{AHP}}$ = 25 mS/cm^2, g_{exc} = 1.2 mS/cm^2, g_{inh} = 1.9 mS/cm^2, E_{Na} = 50 mV, E_{K} = -100 mV, E_{L} = -70 mV, E_{exc} = 0 mV, E_{inh} = -70 mV, β_{m} = -1.2 mV, γ_{m} = 18 mV, β_{w} = -19 mV, γ_{w} = 10 mV, β_{z} = 0 mV, γ_{z} = 2 mV, τ_{a} = 20 ms, ϕ = 0.15, and C = 2 μF/cm^2. These parameter values produce a hybrid operating mode (4). Notably, inclusion of background excitatory and inhibitory synaptic conductance reproduces a "balanced" high-conductance state (2). Surface area was set to 200 μm^2 so that I_{mixed} is reported in pA, like in experiments (see below), rather than as a density.

The mixed signal (I_{mixed}) is the sum of fast (I_{fast}) and slow (I_{slow}) signals. Rather than high- and low-pass filtering a common signal and then combining the outputs (as in **Figs. 2A** and **S1**), we created comparable mixed signals as described below. I_{fast} was generated by convolving a randomly (Poisson) distributed Dirac delta function with a synaptic waveform with a normalized peak amplitude of 1, τ_{rise} = 0.5 ms and τ_{fall} = 3 ms. Fast events occured at a rate of ~1 Hz and were scaled by a_{fast} = 170 pA. I_{slow} was generated using an OU process,

$$\frac{dI_{\mathrm{slow}}}{dt} = -\frac{I_{\mathrm{slow}}(t)-\mu}{\tau} + \sigma\sqrt{\frac{2}{\tau}}\,\xi(t) \qquad \text{(S7)}$$

where ξ is a random number drawn from a Gaussian distribution with 0 average and unit variance, τ = 100 ms to produce a slow-varying random walk with average μ = 30 pA and σ = 120 pA. By generating I_{fast} and I_{slow} independently and summing them to form I_{mixed}, the two components of I_{mixed} are sure to be independent. An OU process with τ = 5 ms, μ = 0 pA, and σ = 1 pA was used to create noisy current (I_{noise}). The same instantiation of I_{mixed} but different instantiations of I_{noise} were applied to all neuron models within a set.

Quantification of signal reconstruction

Reconstruction of the original signal was quantified as coding fraction (CF), as explained in the main text. When synchrony-based demultiplexing was not compared back-to-back with a different decoding strategy (**Fig. 3C**), CF was calculated by comparing the reconstructed fast and slow signals with the original fast and slow signals. In other cases (**Figs. 2C, 3D** and **4B-D**), the reconstructed *mixed* signal was separated into fast and slow components by filtering (see below) so that CF could be measured for each component; in other words, because most decoding strategies reconstruct the mixed signal rather than the individual components, the individual components reconstructed through demultiplexing were added and then separated (the same way as other reconstructed signals were) to prevent differences in CF values from arising through technical differences in how original and reconstructed signals are compared (see **Fig. S3**)

Bayesian Modeling

Bayesian decoding (see main text) requires an encoding model. Parameters of the encoding model were fit to a 20 s-long training set by maximizing the log-likelihood function, $\sum_i R_{\mathrm{obs}}(t)\log\big(\lambda(t)\big) - \lambda(t)$, using the GLM method (5), where $\lambda(t) = \exp(kx + \mu)$ represents the conditional intensity (or instantaneous rate) that depends on a linear filter k, stimulus x, and the cell's baseline log-firing rate μ, and $R_{\mathrm{obs}}(t)$ represents the observed spikes (superimposed from all conductance-based neuron models). In the test set, to estimate $x(t)$, we drew samples $\mathbf{s_i}$ (i=1:1000) from a Gaussian distribution $P(x)$ whose standard deviation was 1× or 0.1× the standard deviation of the true input distribution. The lower standard deviation prevented the encoding model from learning to encode fast stimulus fluctuations (see **Fig. 3D**, light vs. dark green). For each time t, we computed the conditional probability $P(R_{\mathrm{obs}}|s_i)$ to measure the likelihood that the observed population response was generated by stimulus s_i. From Bayes rule, we know that the posterior $P(s_i|R_{\mathrm{obs}})$ is proportional to $P(R_{\mathrm{obs}}|s_i)$. Thus, the Bayes least squares estimate is given by

$$\hat{x}(t) = \frac{\sum_i s_i(t) P\big(R_{\mathrm{obs}}|s_i(t)\big)}{\sum_i P\big(R_{\mathrm{obs}}|s_i(t)\big)}. \tag{S8}$$

SUPPLEMENTARY FIGURES

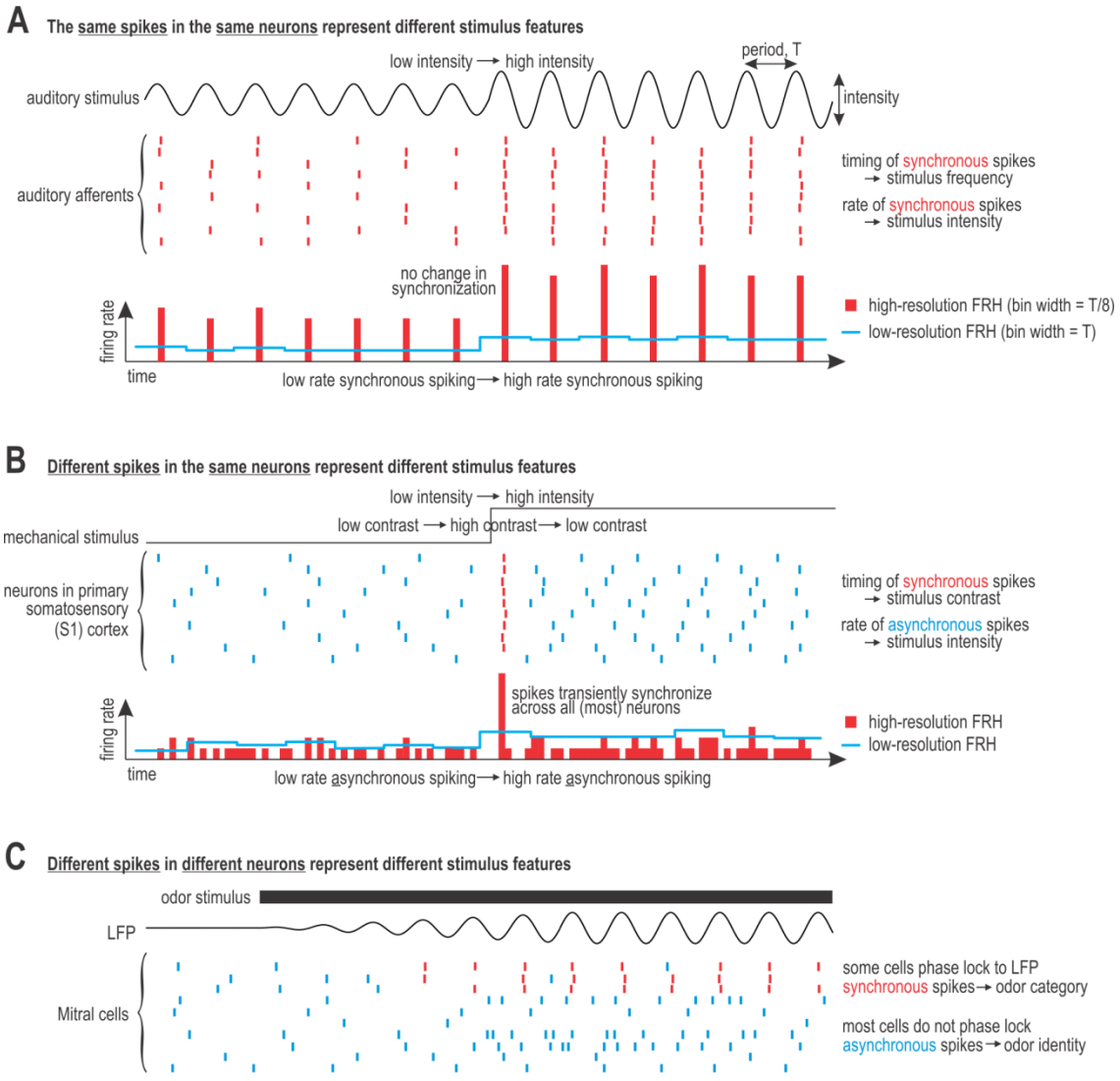

Figure S1. Comparison of multiplexing strategies that use spike rate and timing to represent different stimulus features. Differences boil down to whether rate- and time-based representations comprise the same or different spikes occurring in the same or different neurons. **(A)** In auditory afferents, the same spikes in the same neurons represent different stimulus features. Spikes in all neurons occur at a preferred phase of the periodic stimulus, and thus occur synchronously at an interval reflecting stimulus frequency. But spikes do not occur on every stimulus cycle; instead, their probability varies with stimulus intensity, thus enabling the firing rate to encode stimulus intensity (6). **(B)** In primary somatosensory (S1) cortex, different spikes in the same neurons represent different stimulus features. During low-contrast stimulation, spikes occur asynchronously

at a rate proportional to stimulus intensity. High-contrast features (i.e. abrupt changes in intensity) transiently synchronize spiking across all (most) neurons, enabling synchronous spikes to encode contrast. **(C)** In the olfactory bulb, different spikes in different neurons represent different stimulus features. A small subset of mitral cells phase-lock to network oscillations that develop during an odor; the synchronized spikes occurring in this minority of phase-locked cells encode odor category whereas odor identity is represented by the rate of asynchronous spiking in mitral cells that do not phase-lock (7).

(B vs C) In S1 cortex, each high-contrast stimulus transiently synchronizes spikes across most neurons but spikes occur asynchronously outside those brief (5-10 ms-long) epochs; in other words, transiently synchronized spiking does not preclude asynchronous spiking in the same neuron (as long as high-contrast features are relatively infrequent). Conversely, network oscillations in the olfactory bulb are protracted. If mitral cells produce mostly synchronous spikes while phase-locked, then nearly all asynchronous spikes occur in mitral cells that do not phase lock (see Supplementary Fig. 1 of ref. 8). Phase-locked neurons could conceivably produce asynchronous spikes (e.g. if they fired at rates much higher than the network oscillation frequency), but that does not appear to be the case. At the very least, different mitral cells contribute differentially to time- and rate-based representations depending on how strongly they phase lock, which is unlike the equal contribution of S1 neurons to each code.

(B vs A) In auditory nerve, the number of spikes per stimulus cycle reflect the intensity (envelope) of the periodic input. In S1 cortex, in the absence of a periodic input, asynchronous spikes encode the intensity of the low-contrast (non-synchronizing) input, not the envelope of a synchronizing input. Temporal coding uses synchronized spikes in both cases but whether the rate-based code involves the same or different (synchronous vs. asynchronous) spikes depends on the nature of the stimulus.

In many sensory systems, different stimulus features can be simultaneously encoded using rate- and time-based codes, but there is no one-size-fits-all multiplexing strategy. Instead, whether multiplexed representations involve the same or different spikes occurring in the same or different neurons depends on the stimulus.

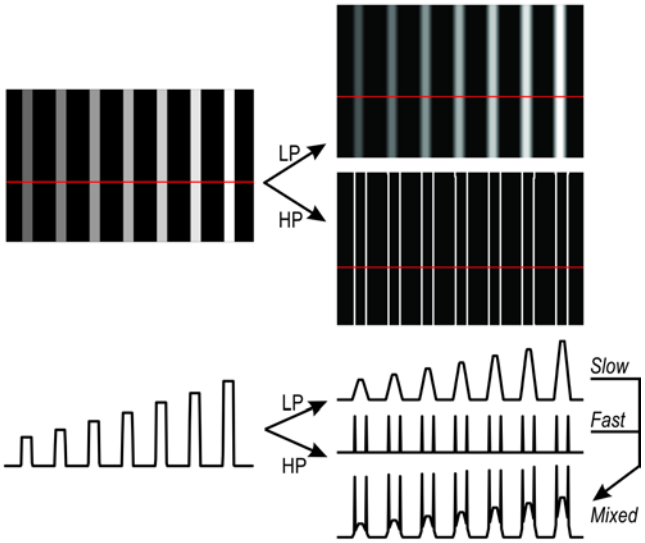

Figure S2. Visual analogue of tactile stimulus used for *in vivo* experiments reported in Figure 1: bars of increasing luminance represents steps of increasing force. Decomposition of this image into first- and second-order stimulus features is shown like in Figure 2A to depict the processing conducted by dichotomously tuned upstream sensory neurons. Neurons at the earliest stage of many sensory pathways behave as low- or high-pass filters such that they spike preferentially to first- or second-order stimulus features, respectively. The eventual re-convergence of pathways carrying information about these stimulus features gives a mixed signal to the neuron(s) of interest.

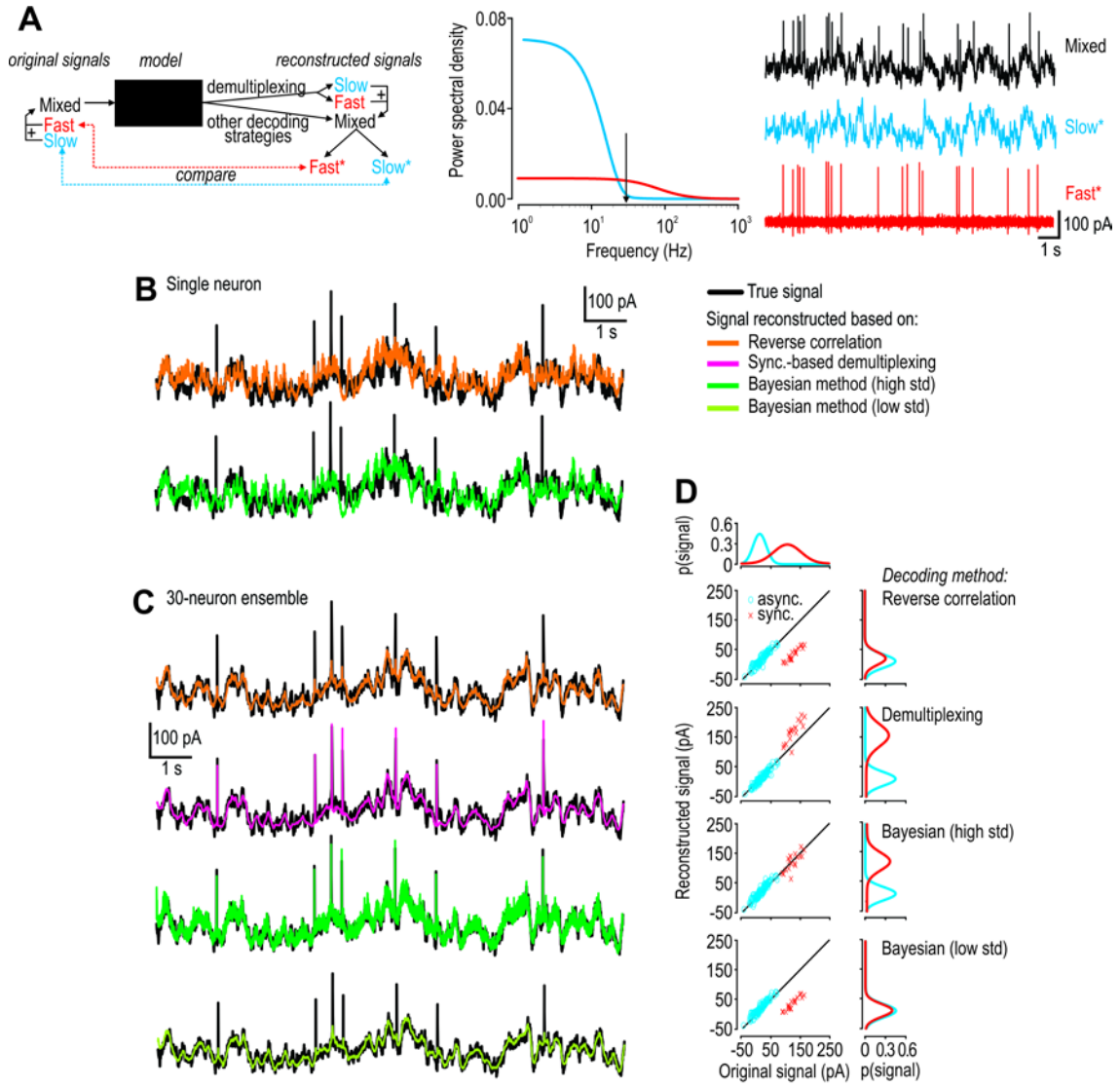

Figure S3. Reconstructing fast and slow components of a mixed signal **(A)**. Left: Schematic shows original signals (left) given to a conductance-based model neuron or ensemble thereof, or to a rate-based model fitted to the output of the conductance-based model neuron(s) (middle), and the signal reconstructed from each model's output (right). Synchrony-based demultiplexing directly reconstructs the fast and slow components whereas all other decoding strategies reconstruct the mixed signal, which must then be split into fast and slow components for comparison with the original fast and slow signals. To make comparison between decoding strategies fair, the fast and slow signals reconstructed through demultiplexing were summed to give a mixed signal that was then split the same way as for all other decoding strategies (except for CF calculations reported in Figure 3C, since there was no comparison across decoding strategies in that case). Fast and slow signals recovered by splitting the mixed signal are marked (*). Middle: Mixed signal was split by

applying a low-pass filter with a 30 Hz cutoff frequency (designed by Matlab R2014b command "designfilt") to isolate the slow signal from the fast signal. Right: Traces show examples of the fast and slow components isolated from a mixed signal using this approach. **(B)** Example of the original mixed signal (black) and its reconstruction from the response of a single neuron using reverse correlation (orange) or Bayesian decoding (green). Both decoding strategies recovered the slow signal but neither recovered the fast signal. See Figure 2C for corresponding CF values. **(C)** Same as B but with reconstructions based on the response of the 30-neuron ensemble. See Figure 3D for corresponding CF values. (**D**) To link discriminability of the fast and slow signals with spike type, local maxima in the original mixed signal were plotted against local maxima in the reconstructed signal using an x or o depending on whether coincident spikes were synchronous or asynchronous, respectively. Distributions of x and o were separable in the original signal (for the stimulus parameters used here) but, for reconstructed signals, this was only true for demultiplexing and Bayesian decoding in which fast events were successfully learned (*i.e.* high standard deviation).

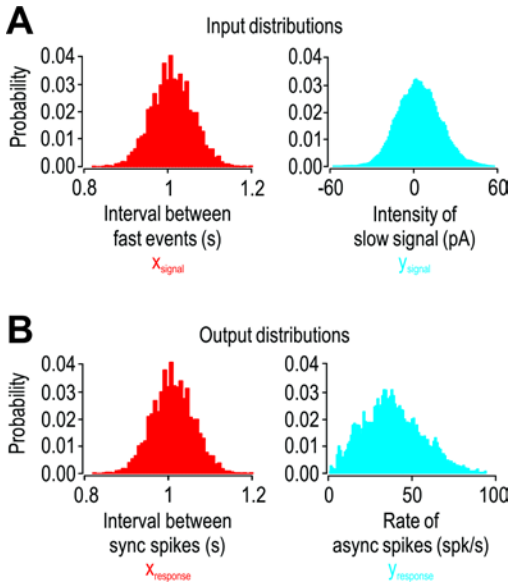

Figure S4. Comparison of the distribution of input **(A)** and output **(B)** measures labeled in Figure 3A. The distribution of intervals between synchronous spikes ($x_{response}$) resembles the distribution of intervals between events in the fast signal (x_{signal}) (red) whereas the distribution of asynchronous spike rate ($y_{response}$) resembles the distribution of intensity of the slow signal (y_{signal}) (blue). This dichotomy is consistent with synchronous and asynchronous spikes forming distinct representations of different features of the mixed signal.

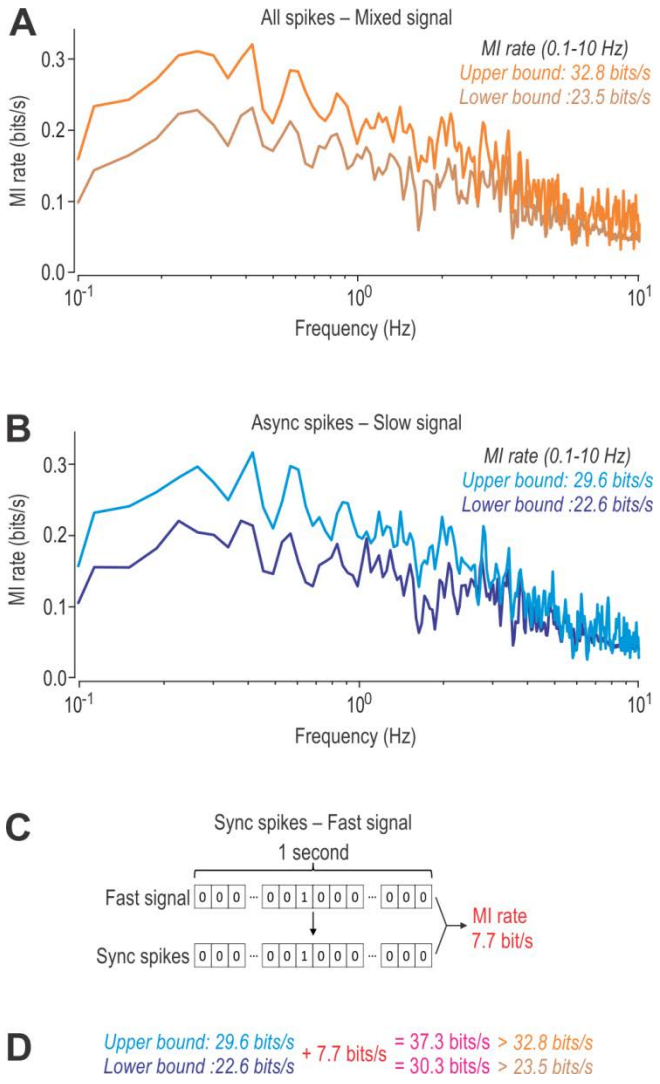

Figure S5. Mutual information (MI) **(A)** between all spikes and the mixed signal, **(B)** between asynchronous spikes and the slow signal, and **(C)** between synchronous spikes and the fast signal. **(D)** The sum of MI calculated in B and C is greater than that calculated in A, thus showing that bandwidth is increased by synchrony-division multiplexing. As a final comparison, we computed the coding efficiency (CE) by normalizing MI by the total entropy of the spike train. When CE equals 1 (ideal case), every variation in the output spike trains corresponds to a unique (distinguishable) change in the input signal (9). For asynchronous spikes, CE can be calculated by normalizing the lower bound of information to its upper bound, which yields $CE_{async} = 0.76$. Note that for synchronous spikes, the total entropy of the spike train does not exceed that of the fast events unless the noise level is unrealistically high ($\sigma_{noise} > 80$ pA, which drives voltage fluctuation with standard deviation $\sigma_V > 16$ mV). Hence, the CE of synchronous spikes is

calculated by normalizing the MI by the total entropy of the fast events (7.9 bit/sec), which yields CE_{sync} = 0.97, which implies that the coding efficiency of synchronous spikes is nearly ideal. The difference in coding efficiency between synchronous and asynchronous spikes reflects the different coding scheme employed by each spike type.

Methods: For panels A and B, the signal was reconstructed and compared against the original signal to determine the reconstruction error, from which the signal-to-noise ratio (SNR) and lower bound of the information rate were computed (10-12)

$$Info_{LB}(R,S) = \int_{cutoff_1}^{cutoff_2} \log_2[1 + SNR(f)]df \tag{S9}$$

$$SNR(f) = \frac{S(f)}{Err(f)} \tag{S10}$$

where $S(f)$ and $Err(f)$ are the Fourier transform of the signal $S(t)$ and the error between the original and reconstructed signals, i.e., $Err(t) = S(t) - S_{est}(t)$. For A, $S(t)$ corresponds to the mixed signal. For B, $S(t)$ corresponds to the slow signal.

The upper bound on mutual information corresponds to trial-to-trial variability in the neural responses to repeated presentations of the same input (13). Given the responses R_i, $i=1, 2, .., L$, obtained from L presentations of the same input $S(t)$ ($L=3$), one can compute the coherence between these responses as

$$CRR(f) = \frac{\frac{1}{L(L-1)} \sum_{i=2}^{L} \sum_{j=1}^{i-1} \left[P_{R_i R_j}(f) \right]}{\left(\frac{1}{L} \sum_{i=1}^{L} \left[P_{R_i R_i}(f) \right] \right)^2} \tag{S11}$$

where C_{RR} (f) is the response-response coherence, P_{RiRj} is the cross-spectrum (Fourier transform of the cross-correlation function) between responses R_i and R_j. The response-response coherence, at each frequency f, represents the strength of correlation between neural responses obtained from repeated presentations of the same input (14). Any trial-to-trial variability in the response to repeated presentations of the same stimulus will decrease the response-response coherence. The upper bound on MI can be estimated from that coherence according to (15-18)

$$Info_{UB}(R,S) = -\int_{cutoff_1}^{cutoff_2} \log_2[1 - \sqrt{C_{RR}(f)}]df \tag{S12}$$

To calculate MI between synchronous spikes and the fast signal in C, the stimulus and response were treated as a series of 0s and 1s where 1s represent time bins in which synchronous

spiking or a fast signal event occurred. A bin size of 5 ms was used throughout. For the stimulus, because the timing of fast events was generated from an independent and identical distribution (i.i.d), the probability of having 1s or 0s is independent across bins; because fast events are sparse (i.e. << than the maximal firing rate), that independence also holds true for the response. The independence across bins enables us to estimate the probability of having 1 or 0 at each bin by counting the number of 1s and 0s during the simulation. Moreover, the joint probability of fast events and synchronous events can be estimated in the same manner. Then, the MI rate between fast-events and synchronous events can be calculated as

$$MI_{\Delta}(R,S) = \sum_{x \in R_{sync}} \sum_{y \in S_{fast}} p(x,y) \log_2 \left(\frac{p(x,y)}{p(x)p(y)} \right) \tag{S13}$$

where R and S represent synchronous spiking and events in the fast signal, respectively, and MI_{Δ} represents the mutual information between two random binary strings in a bin of $\Delta = 5$ ms. Eq.13 can be simplified as

$$MI_{\Delta}(R,S) = \sum_{i \in \{0,1\}} \sum_{j \in \{0,1\}} p(r=i, s=j) \log_2 \left(\frac{p(r=i, s=j)}{p(r=i)p(s=j)} \right) \tag{S14}$$

$$p(z=i) = \sum_{j \in \{0,1\}} p(z=i, y=j) \tag{S15}$$

and z represents r or s. Coding Efficiency (CE) was calculated according to (9)

$$CE = \frac{MI(R,S)}{H(R)} \tag{S16}$$

where $H(R)$ is the total entropy of the spike train (with the same unit as MI).

SUPPLEMENTARY REFERENCES

1. Khubieh A, Ratte S, Lankarany M, & Prescott SA (2016) Regulation of Cortical Dynamic Range by Background Synaptic Noise and Feedforward Inhibition. *Cereb Cortex* 26:3357-3369.
2. Destexhe A, Rudolph M, & Paré D (2003) The high-conductance state of neocortical neurons in vivo. *Nat Rev Neurosci* 4(9):739-751.
3. Morris C & Lecar H (1981) Voltage oscillations in the barnacle giant muscle fiber. *Biophys.J.* 35(1):193-213.
4. Ratté S, Hong S, De Schutter E, & Prescott SA (2013) Impact of neuronal properties on network coding: roles of spike initiation dynamics and robust synchrony transfer. *Neuron* 78(5):758-772.
5. Pillow JW, *et al.* (2008) Spatio-temporal correlations and visual signalling in a complete neuronal population. *Nature* 454(7207):995-999.
6. Wever E & Bray C (1930) Present possibilities for auditory theory. *Psychol Rev* 37:365-380.
7. Friedrich RW, Habermann CJ, & Laurent G (2004) Multiplexing using synchrony in the zebrafish olfactory bulb. *Nat Neurosci* 7(8):862-871.
8. Blumhagen F, *et al.* (2011) Neuronal filtering of multiplexed odour representations. *Nature* 479(7374):493-498.
9. Rieke F, Warland D, de Ruyter van Steveninck RR, & Bialek W (1997) *Spikes: Exploring the Neural Code* (MIT Press, Cambridge, MA).
10. Krahe R, Kreiman G, Gabbiani F, Koch C, & Metzner W (2002) Stimulus encoding and feature extraction by multiple sensory neurons. *J Neurosci* 22(6):2374-2382.
11. Warland DK, Reinagel P, & Meister M (1997) Decoding visual information from a population of retinal ganglion cells. *J Neurophysiol* 78(5):2336-2350.
12. Dan Y, Alonso JM, Usrey WM, & Reid RC (1998) Coding of visual information by precisely correlated spikes in the lateral geniculate nucleus. *Nat Neurosci* 1(6):501-507.
13. Massot C, Chacron MJ, & Cullen KE (2011) Information transmission and detection thresholds in the vestibular nuclei: single neurons vs. population encoding. *J Neurophysiol* 105(4):1798-1814.
14. Roddey JC, Girish B, & Miller JP (2000) Assessing the performance of neural encoding models in the presence of noise. *J Comput Neurosci* 8(2):95-112.
15. Chacron MJ (2006) Nonlinear information processing in a model sensory system. *J Neurophysiol* 95(5):2933-2946.
16. Krahe R, Bastian J, & Chacron MJ (2008) Temporal processing across multiple topographic maps in the electrosensory system. *J Neurophysiol* 100(2):852-867.
17. Marsat G & Pollack GS (2004) Differential temporal coding of rhythmically diverse acoustic signals by a single interneuron. *J Neurophysiol* 92(2):939-948.
18. Middleton JW, Longtin A, Benda J, & Maler L (2009) Postsynaptic receptive field size and spike threshold determine encoding of high-frequency information via sensitivity to synchronous presynaptic activity. *J Neurophysiol* 101(3):1160-1170.